Langmuir

Article

pubs.acs.org/Langmuir

Zwitterion-Coated Iron Oxide Nanoparticles: Surface Chemistry and Intracellular Uptake by Hepatocarcinoma (HepG2) Cells

Sara Mondini,[†,∥] Marianna Leonzino,[‡,∥] Carmelo Drago,[†,⊥] Anna M. Ferretti,[†] Sandro Usseglio,[†] Daniela Maggioni,[§] Paolo Tornese,[‡] Bice Chini,*[,‡] and Alessandro Ponti*[,†]

[†]Laboratorio di Nanotecnologie, Istituto di Scienze e Tecnologie Molecolari, Consiglio Nazionale delle Ricerche, via G. Fantoli 16/15, 20138 Milano, Italy

[‡]Istituto di Neuroscienze, Consiglio Nazionale delle Ricerche, via L. Vanvitelli 32, 20133 Milano, Italy

[§]Dipartimento di Chimica, Università degli Studi di Milano, via C. Golgi 19, 20133 Milano, Italy

Supporting Information

ABSTRACT: Nanoparticles (NPs) have received much attention in recent years for their diverse potential biomedical applications. However, the synthesis of NPs with desired biodistribution and pharmacokinetics is still a major challenge, with NP size and surface chemistry being the main factors determining the behavior of NPs in vivo. Here we report on the surface chemistry and in vitro cellular uptake of magnetic iron oxide NPs coated with zwitterionic dopamine sulfonate (ZDS). ZDS-coated NPs were compared to similar iron oxide NPs coated with PEG-like 2-[2-(2-methoxyethoxy)ethoxy]-acetic acid (MEEA) to investigate how surface chemistry affects their in vitro behavior. ZDS-coated NPs had a very dense coating, guaranteeing high colloidal stability in several aqueous media and negligible interaction with proteins. Treatment of HepG2 cells with increasing doses (2.5−100 μg Fe/mL) of ZDS-coated iron oxide NPs had no effect on cell viability and resulted in a low, dose-dependent NP uptake, inferior than most reported data for the internalization of iron oxide NPs by HepG2 cells. MEEA-coated NPs were scarcely stable and formed micrometer-sized aggregates in aqueous media. They decreased cell viability for dose ≥50 μg Fe/mL, and were more efficiently internalized than ZDS-coated NPs. In conclusion, our data indicate that the ZDS layer prevented both aggregation and sedimentation of iron oxide NPs and formed a biocompatible coating that did not display any biocorona effect. The very low cellular uptake of ZDS-coated iron NPs can be useful to achieve highly selective targeting upon specific functionalization.

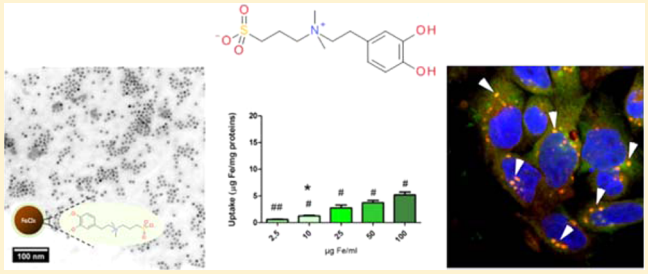

1. INTRODUCTION

Though concerns have been raised about the possible dangers related to the effects of nanoparticles (NPs) in living organisms,[1] a large share of the research on NPs is in the biomedical field.[2] In this paper, we focus on NPs consisting of an inorganic crystalline core (nanocrystal) coated with a layer of chemically bound organic molecules (ligands). Such NPs have two major appealing features for biomedicine: (i) the inorganic core can be tuned to have useful diagnostic/therapeutic properties, and (ii) the organic coating can be engineered to endow the NPs with desired colloidal stability, targeting capability, pharmacokinetics, and additional diagnostic/therapeutic functions.[3] Size and surface chemistry are the main factors determining the in vivo behavior of NPs. For instance, quantum dots with diameter $d \leq 5$ nm undergo renal excretion,[4,5] whereas NPs with $d \geq 100$ nm are quickly captured by the mononuclear phagocyte system (MPS).[6] Surface chemistry is relevant because it mediates all interactions of the NPs with the environment. As an example, iron oxide NPs with positive surface charge displayed a 100-fold larger uptake by CNS cells than negatively charged NPs.[7] The role of surface chemistry in regulating protein adsorption onto NPs cannot be underestimated. Several phenomena may adversely affect the effective use of NPs in a living organism, but protein adsorption in the bloodstream, leading to the formation of a biocorona surrounding the NPs,[8] is a major one. The biocorona increases the NP diameter, hampers the NP targeting capability, affects interaction with cells, and promotes recognition by the MPS, which clears the NPs from the bloodstream by size-dependent engulfment mechanisms.[9] Up to now, the most widely employed approach to have good colloidal stability, counter biocorona formation, and increase circulation time has been coating the NPs with biocompatible polyethylene glycol (PEG).[10] However, PEG coating significantly adds to the NP diameter, for example, coating 13 nm iron oxide nanocrystals with a PEG_{5000} derivative led to NPs with a hydrodynamic diameter of 50 nm.[11] Such increase can prevent renal excretion of NPs and lead to their accumulation in the organism. The

Received: April 23, 2015
Revised: June 4, 2015
Published: June 9, 2015

DOI: 10.1021/acs.langmuir.5b01496
Langmuir 2015, 31, 7381−7390

Scheme 1[a]

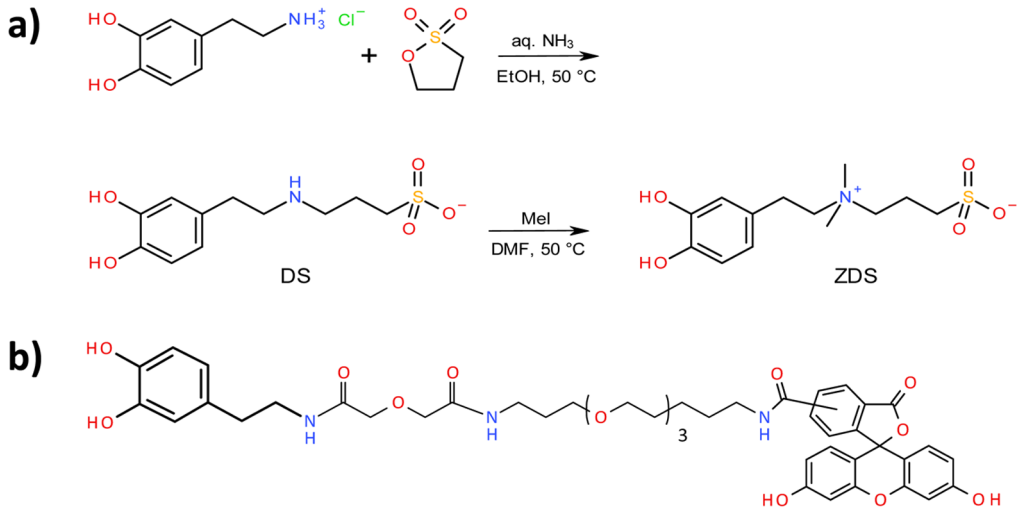

[a](a) Synthesis of zwitterionic dopamine sulfonate (ZDS) via dopamine sulfonate (DS). (b) Structure of the fluorescent catecholic ligand (FCL).

PEG chains may also entrap bioactive moieties present on the NP surface and hinder their presentation to the environment.

Recently, zwitterions have attracted much attention as biocompatible coatings as witnessed by two review articles.[3,12] Three types of zwitterionic groups have been employed, namely, carboxybetaine, phosphocholine, and sulfobetaine. We decided to investigate the latter type of zwitterion since sulfobetaines may have reduced aspecific protein adsorption[12,13] and do not alter the water H-bonding structure.[14] As inorganic core, we focused on magnetic iron oxide nanocrystals since they have wide potential in applications such as drug delivery, gene therapy, magnetic resonance imaging (MRI), hyperthermia, and cell tracking.[15−18] Iron oxide NPs coated with polymeric sulfobetaines have already been reported,[19,20] but we are interested in small zwitterions able to coat NPs without increasing their diameter by more than a few nanometers. In addition to oleic-acid-coated iron oxide NPs stabilized by a physisorbed layer of zwitterionic ASB-14,[21] iron oxide NPs grafted with small sulfobetaines were recently reported.[22,23] In the latter cases, the sulfobetaine coating was just ca. 2 nm thick. Iron oxide NPs coated with a sulfobetaine siloxane shell[22] were shown to be colloidally stable in physiological conditions and showed no aggregation in phosphate buffered saline (PBS) with 50% fetal bovine serum (FBS) for 24 h.[24] Zwitterionic dopamine sulfonate (ZDS) was also used to coat iron oxide NPs,[23] which displayed good colloidal stability and reduced protein adsorption both in PBS with 10% FBS and in vivo, as determined by size exclusion chromatography (SEC).[25] Uptake of ZDS-coated iron oxide NPs by HeLa cells was deemed low on the basis of Prussian blue staining. ZDS-coated iron oxide NPs were shown by MRI to undergo both renal excretion and liver accumulation in mice.[26]

We considered that magnetic ZDS-coated iron oxide NPs are a promising nanosystem for biomedical applications. The small thickness of the ZDS coating offers the possibility to modulate size-dependent properties by varying the nanocrystal size (and shape) resorting to the well-developed techniques of nanocrystal chemistry[27−29] in addition to the lack of steric effects that can adversely affect the effectiveness of grafted functional molecules. To synthesize nanosystems useful for biomedicine, it is necessary to investigate the interaction of ZDS-coated iron oxide NPs with cells as to their cytotoxicity, internalization, and intracellular fate. In this paper, we report the results of such an investigation along with a detailed characterization of the ZDS coating structure, obtained by Fourier transform infrared (FTIR) spectroscopy and thermal gravimetric analysis (TGA), and about the protein adsorption onto the NPs, obtained by dynamic light scattering (DLS) experiments. For the in vitro investigation, we chose the human liver hepatocellular carcinoma cell line HepG2 for its high phagocytic activity. HepG2 cells were previously used to evaluate the biocompatibility and uptake of iron oxide NPs with different coating.[30−35] To investigate the intracellular fate of NPs, we used iron oxide NPs coated with a mixture of ZDS and a fluorescein derivative (FLC) possessing a catecholic terminal for grafting to the NPs.

In addition to zwitterionic NPs, we also investigated iron oxide NPs coated with 2-[2-(2-methoxyethoxy)ethoxy acid (MEEA). MEEA is a commercially available, water miscible, PEG-like carboxylic acid, which binds to the iron oxide NP surface as carboxylate anion.[36] Since MEEA and ZDS are expected to form coating of equal thickness (the two molecules have similar size) and since we used a single batch of monodisperse iron oxide nanocrystals for all NP types, ZDS- and MEEA-coated NPs could only differ by their surface chemistry.

2. EXPERIMENTAL SECTION

2.1. Materials. All chemicals were purchased from Sigma-Aldrich and used as received without further purification. Concentrated HNO_3 and HCl used for NP digestion were Aldrich Trace Select reagents. Deionized (DI) water was prepared using a Milli-Q Plus water purification system (resistivity >18.2 mΩ cm at 25 °C). HepG2 cells (a human hepatocarcinoma cell line) were from American Type Culture Collection.

2.2. Synthesis of Iron Oxide Nanoparticles. Magnetic iron oxide NPs ($d \approx 9$ nm) were synthesized according to a modification of a literature procedure[37] that is detailed in the Supporting Information. Larger ($d \approx 12$ nm) iron oxide NPs were prepared in ODE according to a slight modification of a recently developed procedure[38] adjusting the $Fe(CO)_5$:OlAc molar ratio to 3:1.

2.3. Synthesis of Ligands. The synthesis of zwitterionic dopamine sulfonate (ZDS) was carried out according to a modification

DOI: 10.1021/acs.langmuir.5b01496
Langmuir 2015, 31, 7381−7390

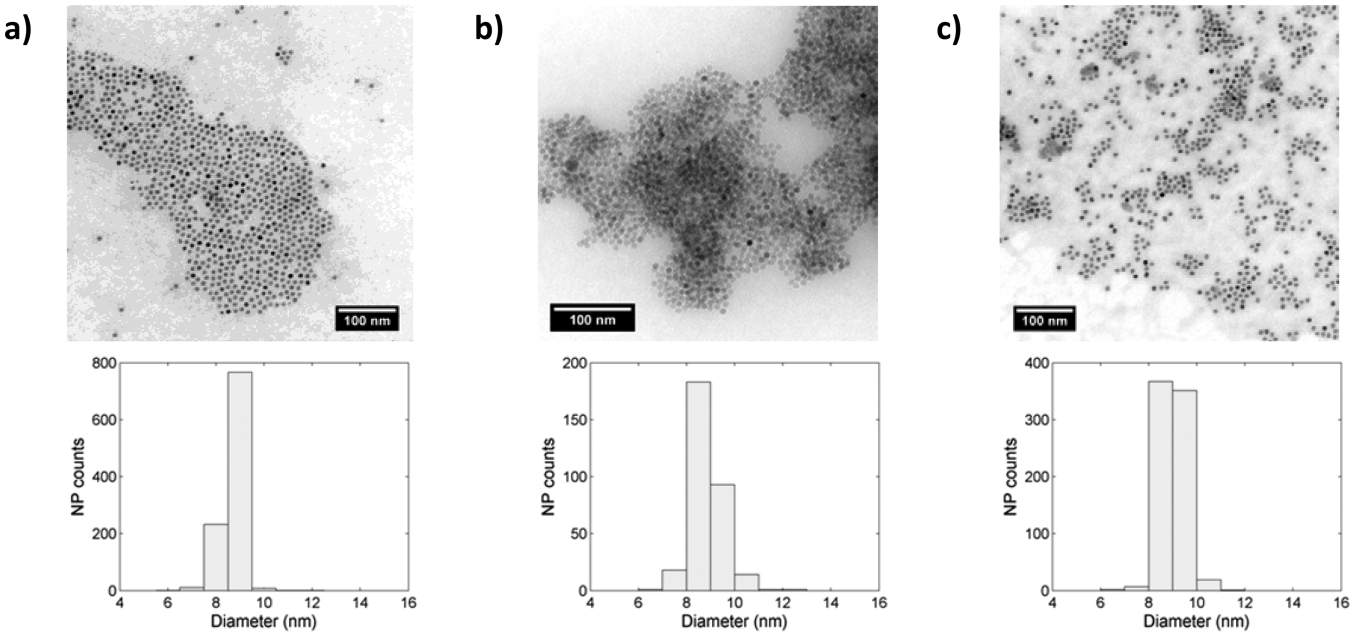

Figure 1. TEM image of OlAc- (a), MEEA- (b), and ZDS-coated (c) iron oxide NPs along with the corresponding distribution of the diameter of the nanocrystal core obtained by the software Pebbles.[43] (Additional TEM images can be found in the Supporting Information.)

of a previously reported procedure (Scheme 1a).[39] See the Supporting Information for further detail. The fluorescent catecholic ligand (FCL, Scheme 1b) was synthesized following the pathway detailed in the Supporting Information.

2.4. Ligand Exchange of Iron Oxide Nanoparticles. We replaced the oleic acid coating of iron oxide NPs with either MEEA or ZDS by a two-step ligand exchange procedure illustrated in ref 39. Fluorescent iron oxide NPs (coated with a mixture of ZDS and FLC) were prepared by a different two-step procedure. First, dry OlAc-coated iron oxide NPs (0.804 mg) were treated with a solution of FLC (5 mg) in methanol (1 mL). The mixture was gently stirred at 45 °C for 6 days. Second, the NPs were treated with a solution of ZDS (5 mg) in DMF/water 8:5 (1.3 mL) and the mixture was stirred at 70 °C for 16 h. The NPs were precipitated by adding acetone, redispersed in DI water, and purified from the excess ligands by dialysis against DI water (MWCO 12.5 kDa, 48 h).

2.5. Cell Cultures. HepG2 cells, a cell line from human hepatocarcinoma, were grown in RPMI medium supplemented with 2 mM L-glutamine, 100 U/mL Pen/Strep, 1 mM sodium pyruvate, and 10% FBS (Sigma-Aldrich) and maintained at 37 °C, in humidified atmosphere with 5% CO_2.

2.6. Cytotoxicity Assay. Cytotoxicity of iron oxide NPs was evaluated with a colorimetric method that assesses the metabolic activity of cells by measuring the reduction of [3-(4,5-dimethylthiazol-2-yl)-5-(3-carboxymethoxyphenyl)-2-(4-sulfophenyl)-2*H*-tetrazolium] (MTS) (CellTiter 96 AQueous One Solution Cell Proliferation Assay, Promega). Experiments were carried out in the log phase of growth after the cells had been seeded in 24-well plates (35 000 cells/cm^2) and allowed to adhere for 24 h. NPs were added to the medium as water dispersions to final concentrations of 2.5, 5, 10, 25, 50, and 100 μg Fe/mL, and the cells were exposed to NPs for 24 h. All treatments were performed in quintuplicate. Cell viability was expressed as the percentage difference between treated and untreated cells (set at 100%).

2.7. Prussian Blue Staining and Imaging. HepG2 cells were seeded on 24 mm glass coverslips (52 000/cm^2) the day before NP exposure. NP dispersions were added to a final volume of 2 mL of culture medium at the indicated final concentration. After 24 h, exposure was stopped by removing all noninternalized NPs by extensive PBS washing and fixed for 30 min in 4% paraformaldehyde (PFA). For Prussian Blue staining, coverslips were then incubated for 30 min with freshly prepared Perls' reagent (4% potassium ferrocyanide/12% HCl, 1:1 v/v), washed in PBS, and mounted onto microscope slides. Bright-field images were acquired at 63× magnification using an optical microscope (Axioplan, Zeiss) coupled to a CCD camera (AxioCam, Zeiss). Cells exposed to fluorescent NPs were stained with 4′,6-diamidino-2-phenylindole (DAPI) after fixation and mounted onto microscope slides. For Lysotracker labeling, after 6 or 24 h of NPs exposure, NPs-containing medium was removed and substituted with fresh medium containing 1 μM Lysotracker-Red (Molecular Probes). Cells were incubated for 30 min in the dark at 37 °C, then washed with PBS and fixed with 4% PFA. Coverslips were stained with DAPI and mounted onto microscope slides. All fluorescent slides were imaged with a confocal microscope (LSM 510 Meta, Zeiss) under a 63× magnification objective.

2.8. Quantification of NP Uptake by HepG2 Cells. HepG2 cells were seeded on 10 cm plates, 45 000/cm^2, for 24 h and exposed to NP dispersed in culture medium to a final concentration of 0, 2.5, 10, 25, 50, or 100 μg Fe/mL for 24 h. The cells were then washed five times with PBS to remove all uninternalized NPs, detached from plates by trypsin treatment, and collected by centrifugation (5 min, 800*g*). We cannot exclude that, after this treatment, some NPs can still be present outside the cells (i.e., tightly adhering to the plasma membrane); however, because fluorecently labeled NPs did not stain the plasma membrane (see Figures 7 and 8), we estimated this fraction to be not quantitatively relevant. After centrifugation, pellets were resuspended in distilled water and protein content was measured via the BIORAD-Dc protein assay. The cell pellets were digested and treated with tiron at pH ≅ 7 to form the red complex $[Fe(tiron)_3]^{3-}$ that was spectrophotometrically quantified[40] (see the Supporting Information). At variance with a previously reported method,[41] we did not rely on the absorbance at a single wavelength but exploited the full spectral information content.[42]

3. RESULTS AND DISCUSSION

3.1. Synthesis of Iron Oxide NPs. Monodisperse spherical OlAc-coated iron oxide nanocrystals (Figure 1a) were synthesized by a literature solvothermal procedure.[37] The median diameter $\langle d \rangle$ = 8.7 nm, and the diameter standard deviation σ_d = 0.4 nm, resulting in a very low dispersion $\sigma_d/\langle d \rangle$ = 4.6%. The electron diffraction pattern (see the Supporting Information) is in agreement with that of bulk magnetite. However, due to the small size of the nanocrystals and the

DOI: 10.1021/acs.langmuir.5b01496
Langmuir 2015, 31, 7381−7390

Scheme 2. Ligand Exchange Procedure Leading to Iron Oxide NPs Coated with MEEA, ZDS, and a Mixture of ZDS and FLC

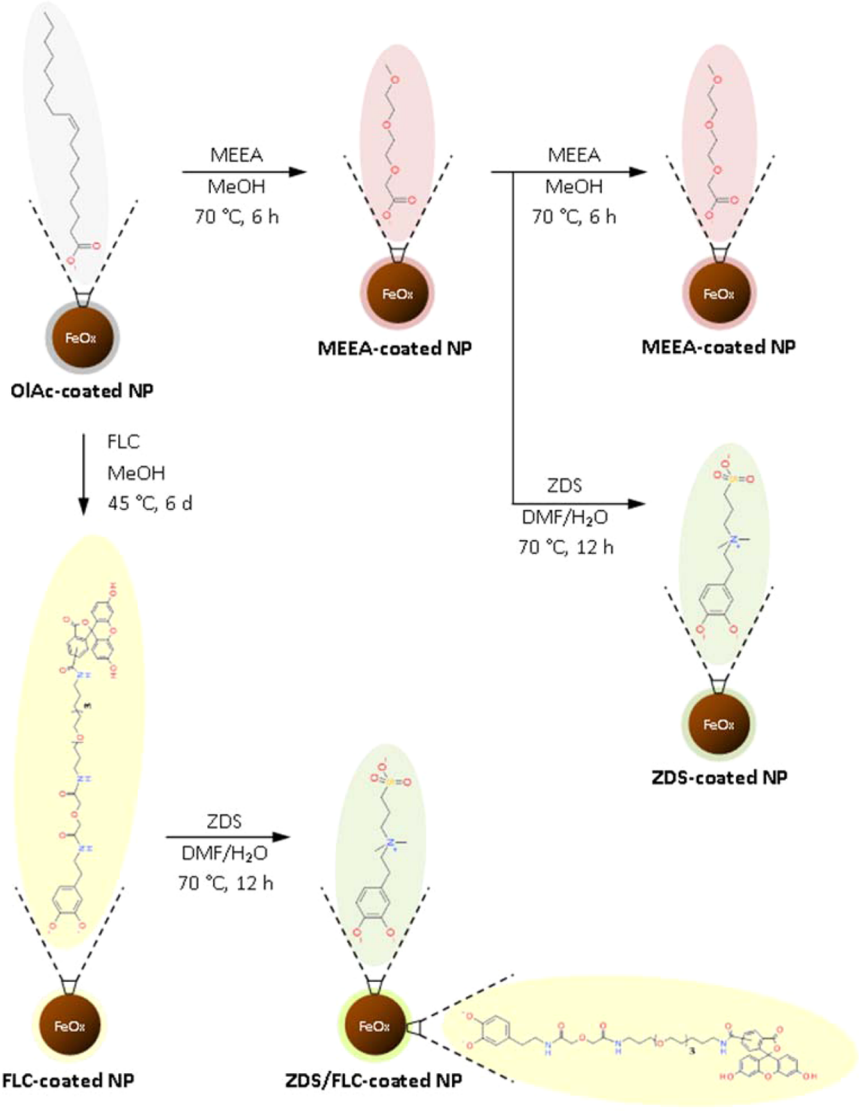

similarity of the magnetite and maghemite crystal structures, we can at most conclude that they are iron oxide nanocrystals with spinel structure and stoichiometry between Fe_3O_4 and Fe_2O_3. From this batch of iron oxide nanocrystals, we prepared NPs coated with MEEA, ZDS, and a mixture of ZDS and the fluorescein derivative FLC by ligand-exchange procedures (Scheme 2). MEEA- and ZDS-coated NPS were synthesized by a literature procedure[39] followed by purification by dialysis (Figure 1b,c). The parameters of the core diameter distribution were $\langle d \rangle$ = 8.8 nm, σ_d = 0.6 nm, and $\sigma_d/\langle d \rangle$ = 7.3% for MEEA-coated NPs and $\langle d \rangle$ = 9.0 nm, σ_d = 0.5 nm, and $\sigma_d/\langle d \rangle$ = 5.2% for ZDS-coated-NPs. Fluorescent iron oxide NPs were obtained by coating the nanocrystals with a mixture of FLC and ZDS by a different two-step procedure. The parameters of the core diameter distribution after ligand exchange were $\langle d \rangle$ = 8.1 nm, σ_d = 0.8 nm, and $\sigma_d/\langle d \rangle$ = 9.4%. (See the Supporting Information for additional TEM images.)

3.2. Characterization of NP Coating. As surface chemistry is a major factor influencing the NP interaction with cells, we investigated in some detail the coating of the various NP types. FTIR spectra of OlAc-, MEEA-, and ZDS-coated iron oxide NPs are pictured in Figure 2a, while the spectra of the free ligands are available in the Supporting Information. The spectrum of OlAc-coated NPs features prominent C−H stretching (2954, 2919, and 2850 cm^{-1}) and carboxylate stretching (1550 and 1463 cm^{-1}) peaks. The spectrum of MEEA-coated NPs shows weak C−H (2956, 2923, and 2855 cm^{-1}), carboxylate (1634 and 1410 cm^{-1}), and C−O−C (1200 and 1100 cm^{-1}) stretching peaks typical of MEEA.[36] In addition to weak C−H peaks (2850−2950 cm^{-1}), the spectrum of ZDS-coated NPs is rich with diagnostic peaks such as the S−O stretching peak (1209 cm^{-1}),[11] the C−H deformation peaks of the dimethylammonium moiety (1496 and 1042 cm^{-1}),[44] and the ring stretching (1596 cm^{-1}) and C−H deformation (914−732 cm^{-1}) peaks of 1,2,4-trisubstituted benzenes. This spectrum is similar to that reported for iron oxide NPs coated with a short siloxane sulfobetaine.[22]

Both types of NP were subjected to TGA (Figure 2b) by heating in air up to 1000 °C. The percentage weight loss of MEEA-coated NPs (16.5%) is close to that previously observed[36] and corresponds to a coating density of (6.1 ± 0.3) molecules/nm^2, not far from the literature data (4.2−4.7 molecules/nm^2) for similarly sized aliphatic carboxylic acids.[45] The TGA profile of ZDS-coated NPs displays two weight

DOI: 10.1021/acs.langmuir.5b01496
Langmuir 2015, 31, 7381−7390

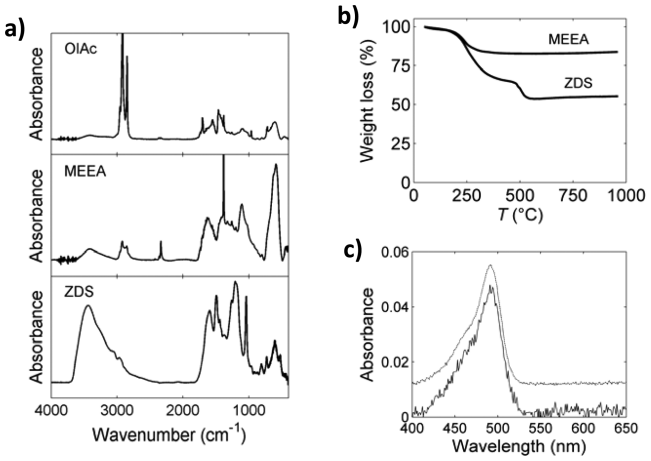

Figure 2. Characterization of NP coating. (a) FTIR spectra of OlAc- (top), MEEA- (middle), and ZDS-coated (bottom) iron oxide NPs; the narrow peak at 1384 cm^{-1} is due to an hexane impurity. (b) TGA of MEEA- and ZDS-coated iron oxide NPs. (c) UV–vis spectra of ZDS/FLC-coated iron oxide NPs (solid line) compared with the spectrum of 5(6)-carboxyfluorescein (dotted line, shifted upward by 0.012 absorbance units for the sake of clarity).

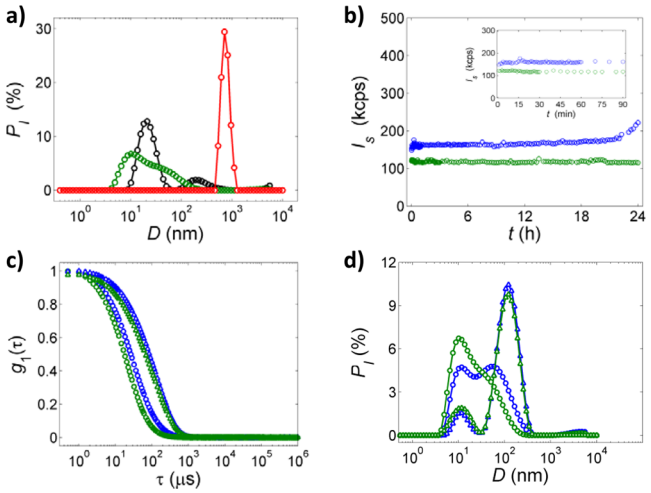

Figure 3. DLS of MEEA- and ZDS-coated iron oxide NPs. (a) Intensity-weighted diameter distribution P_I of dispersions of MEEA- (red) and ZDS-coated (black) NPs in deionized water; P_I of the cell culture medum (green) is also shown. (b–d) Comparison of ZDS-coated NPs in cell culture medium (blue) and pure cell culture medium (green): (b) scattered intensity I_s as a function of time t, the inset shows the initial behavior; (c) normalized first-order autocorrelograms $g_1(\tau)$; (d) intensity-weighted distribution P_I. In panels (c) and (d), circles and triangles denote data at 0 and 24 h, respectively.

losses: 33% in the 100–440 °C range followed by 12% in the 440–580 °C range. The first can be ascribed to the loss of the aliphatic part of the ZDS molecule while the second to the combustion of the remaining aromatic part. This attribution is supported by literature examples[46–48] and by considering that the aliphatic:aromatic weight ratio for ZDS is close to 3:1. The total weight loss of ZDS-coated NPs (45%) corresponds to a coating density of (15.5 ± 0.9) molecules/nm^2, much larger than that of short siloxane sulfobetaine ligands on iron oxide NPs (6.3 molecules/nm^2).[22] Such high value is similar to that observed for OlAc/ABS-14 bilayer iron oxide NPs[21] suggesting that a ZDS/ZDS bilayer might be present.

The ZDS/FLC mixed coating of iron oxide NPs was investigated by UV–visible spectroscopy (Figure 2c). After purification, the absorption spectrum of the ZDS/FLC NPs closely corresponded to that of the 5(6)-carboxyfluorescein chromophore of FLC, confirming that the treatment with ZDS, needed to endow the fluorescent NPs with colloidal stability in water, was successful and ZDS/FLC mixed coating was finally achieved. Quantitative analysis of the UV–vis spectrum allowed us to estimate the number of FLC molecules anchored to a NP to be around (4.0 ± 0.2) × 10^2. This value can be considered reasonable compared with the (3.1 ± 0.2) × 10^3 ZDS molecules per NP estimated from the above TGA data.

3.3. Nanoparticle Colloidal Stability. The colloidal stability of the NPs and the protein adsorption in the complete cell culture medium were investigated by DLS. Intensity-weighted size distributions P_I are shown in Figure 3, and volume-weighted size distributions P_V can be found in the Supporting Information. The colloidal state of MEEA- and ZDS-coated NPs was first studied in deionized water (Figure 3a). MEEA-coated NPs displayed a single peak in both P_I and P_V with mean diameter $D_I \cong D_V \cong 750$ nm. It is clear that these NPs were present in deionized water as aggregates (cf. Figure 1b). ZDS-coated NPs have a major peak in P_I at $D_I = 23$ nm (85%) and a minor peak at $D_I = 240$ nm (15%). The major peak size $D_V = 12$ nm is in good agreement with literature values[25] and shows that the ZDS coating is less than 2 nm thick. Despite most of the ZDS-coated NPs being well dispersed, some aggregates are present in deionized water, which however represent a minor fraction of the NP mass as evidenced by the peak area ratio of both P_I (85:15) and P_V (99:1). Although ZDS is globally neutral, the zeta potential of ZDS-coated NPs in deionized water was negative, $\zeta = -8.6$ mV, as previously reported for quantum dots coated with a polymer bearing sulfobetaine pendant groups (−13.1 mV)[49] and gold NPs coated with sulfobetaine zwitterionic ligands (−17.9/−14.8 mV).[13]

The behavior of ZDS-coated NPs dispersed in the complete cell culture medium was monitored at the concentration and for the time interval used in the cellular uptake experiments (see below) and compared to that of the pure cell culture medium. The scattered light intensity I_s (Figure 3b) was constant in the whole interval for the cell culture medium whereas for ZDS-coated NPs dispersed in cell culture medium a small increase was only observed at longer times, particularly in the 21–24 h range, indicating a good stability of the examined dispersions. These findings are further supported by the volume-weighted size distributions P_V that did not display significant changes over 24 h. However, inspection of the first-order autocorrelograms $g_1(\tau)$ and intensity-weighted size distributions P_I (Figure 3c, d) shows that an increase of the intensity-weighted size occurred after 24 h. Recalling that I_s and P_I are very sensitive to size changes (I_s, $P_I \propto D^6$), the aggregation occurring after 24 h can be considered of lesser importance. It is also worth noting that this variation can be ascribed to changes occurring in the medium during time, as the autocorrelation function $g_1(\tau)$ and P_I curve are similar irrespective of the presence of NPs. These data show that fast protein adsorption, which develops in a few minutes after contacting and leads to multifold increase in I_s,[50] did not occur. However, slow protein adsorption and/or NP aggregation due to slow ligand desorption cannot be excluded.

Since the interpretation of DLS data can be not completely reliable because the data inversion from the time domain to the

DOI: 10.1021/acs.langmuir.5b01496
Langmuir 2015, 31, 7381–7390

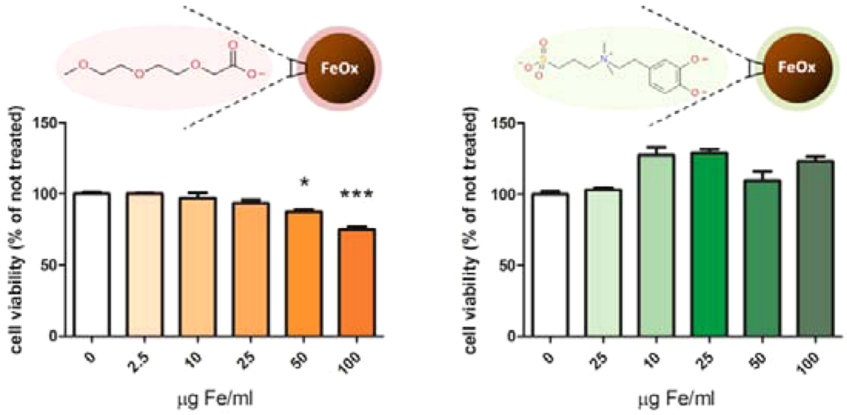

Figure 4. Cell viability upon exposure to nanoparticles. HepG2 cells were exposed for 24 h to increasing concentrations of MEEA- (left) or ZDS-coated (right) NPs, then extensively washed and processed for MTS cell viability assay. Cell viability was calculated as percentage of not treated cells values. Obtained data are presented as mean ± SEM and compared to control values using ANOVA test. *$p < 0.05$; ***$p < 0.001$.

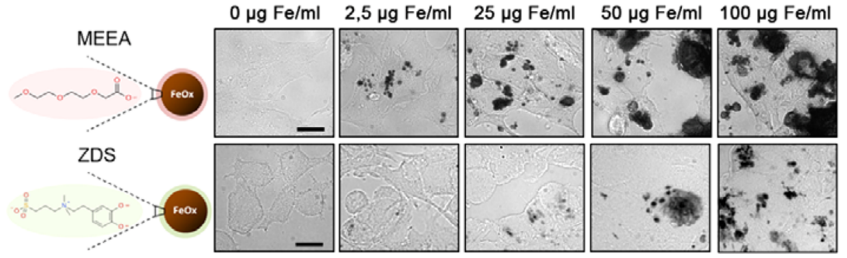

Figure 5. Prussian Blue staining of nanoparticles internalization by HepG2 cells. HepG2 cells were exposed for 24 h to different concentrations of MEEA- (top) or ZDS-coated (bottom) NPs, washed and processed for Prussian Blue staining and optical imaging. Black aggregates indicate the presence of iron. Scale bar = 10 μm.

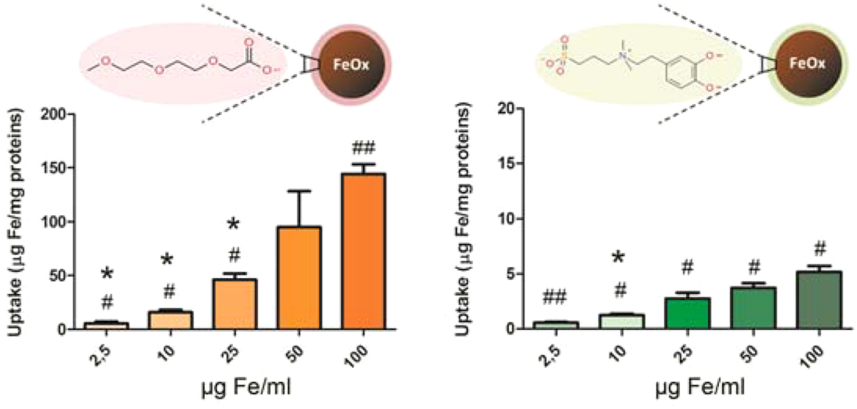

Figure 6. Nanoparticle internalization in HepG2 cells after 24 h incubation with increasing concentrations of MEEA- (left) or ZDS-coated (right) NPs. Note the different vertical scales in the panels. Results are presented as mean ± SEM, and their significance was assessed using Student's t test, after testing for equal variance using the F-test. Student's t test was applied to test for uptake differences between adjacent doses (*) and with respect to the control (#). *$p < 0.05$; $^{\#}p < 0.05$, $^{\#\#}p < 0.005$.

size domain is an ill-posed problem,[51] we repeated (and enlarged) the DLS investigation employing monodisperse ZDS-coated NPS with slightly larger core size ($\langle d \rangle$ = 12.1 nm, σ_d = 0.7 nm, and $\sigma_d/\langle d \rangle$ = 5.8%; see the Supporting Information). The results confirmed the conclusion drawn above. In serum-free media, these NPs had D_I = 19−23 nm and D_V = 15 nm (deionized water, PBS, RPMI) and were colloidally stable for 24 h (RPMI); minor aggregation was observed in P_I. DLS experiments on dispersions of these ZDS-coated NPs in complete cell culture medium and in PBS 1× added with 10% FBS confirmed the absence of protein adsorption and the substantial colloidal stability after 24 h.

3.4. Cytotoxicity and Internalization of Iron Oxide NP in HepG2 Cells. To investigate the cytotoxicity and the intracellular uptake of NPs, HepG2 cells were treated for 24 h with MEEA- or ZDS-coated NPs dispersed in the cell culture medium at various concentrations (2.5−100 μg Fe/mL; see Supporting Information for dose expressed in other units). The addition of NPs was such not to significantly perturb the pH and osmolarity of the culture medium. Cell viability upon NP exposure was measured by an MTS-based colorimetric assay. The highest doses of MEEA-coated NPs (50 and 100 μg Fe/mL) produced a small cytotoxic effect (Figure 4a). On the contrary, no cytotoxicity was observed for ZDS-coated NPs

DOI: 10.1021/acs.langmuir.5b01496
Langmuir 2015, 31, 7381−7390

even at the highest dose (Figure 4b). It is to note here that at the highest NP concentration used in this study (100 μg/mL), iron does not interfere with the MTS assay.[52]

Qualitative observation of NPs uptake by HepG2 cells by Prussian Blue staining revealed that this process is dose-dependent for both MEEA- and ZDS-coated NPs (Figure 5). Clearly, MEEA-coated NPs were internalized in higher amount than ZDS-coated NPs.

The investigation of NP uptake was put on a quantitative basis by spectrophotometric measurement of the cellular iron content. The NP uptake was evaluated by calculating the iron uptake as $U = (m_{Fe}/m_{protein})_{treated} - (m_{Fe}/m_{protein})_{control}$, where m_{Fe} and $m_{protein}$ are the cellular iron and protein mass measured after 24 h treatment and averaged over the replicates. [The intrinsic iron content of control HepG2 cells was $(m_{Fe}/m_{protein})_{control} = (0.4 \pm 0.1)\ \mu g_{Fe}/mg_{protein}$.]

In Figure 6 the iron uptake U is reported for MEEA- and ZDS-coated NPs. (See the Supporting Information for uptake expressed in alternate units). For both NP types, the uptake after 24 h is dose-dependent with an exponential approach to saturation (see the Supporting Information). The uptake of MEEA-coated NPs was 20−30 times higher than that of ZDS-coated NPs. Both core and coating size are equal in MEEA- and ZDS-coated NPs, so surface chemistry is likely the only one responsible for the unequal uptake. The chemical nature of the coating (zwitterionic vs neutral) might have affected the interaction between NPs and cells, but it primarily influenced the NP colloidal stability. Low coating density led to poor colloidal stability of MEEA-coated NPs so that cells came in contact with aggregated MEEA-coated NPs and, as previously shown,[50] displayed high uptake of these aggregates. Furthermore, MEEA-coated NPs sedimented during the experiments so that cells were exposed to a local NP concentration higher that the nominal one. Conversely, high coating density, lack of protein adsorption, and nondisruption of the H-bonding structure of water[12] allowed the cells to interact with well-dispersed ZDS-coated NPs and led to low internalization.

Since studies about the internalization of NPs in cells widely differ as to the type of cell and NP (composition, morphology, surface chemistry) and treatment conditions (dose, duration, etc.),[53] care must be exercised in comparing literature data, in particular data from less recent experiments where parameters such as NP sedimentation and protein absorption might have not been properly considered.[54] With this caveat in mind, we now compare uptake of 9 nm ZDS- and MEEA-coated iron oxide NPs by HepG2 cells with literature data. We first focus on uptake data of iron oxide NPs by HepG2 cells. Except for a single case, uptake falls between those observed by us for ZDS-coated and MEEA-coated NPs. Uptake of the latter is higher than (but comparable to) that reported for cationic and galactose-decorated magnetoliposomes,[30] iron oxide NPs decorated with glucosamic acid[55] or aminopropylsiloxane moieties,[34] and commercial "anionic" NPs.[35] In these cases, the NPs formed aggregates. The uptake of ZDS-coated NPs is lower than (but comparable to) that observed for well dispersed iron oxide NPs coated with PEG_{600} carboxylic acid[34] and for anionic magnetoliposomes.[30] Iron oxide NPs (11 nm) coated with dimercaptosuccinic acid showed slightly lower uptake with respect to our ZDS-coated NPs.[31]

Second, we compare our results with the scarce uptake data for iron oxide NPs with zwitterionic coating. In both cases, we found that NPs had a polymeric coating bearing carboxybetaines. In one case,[19] NPs were coated with poly(acrylic acid) functionalized with ammonium groups and were well dispersed (D = 19 nm) when fed to RAW 264.7 cells. In the other case,[20] a polycarboxybetainemethacrylate polymer was used to coat iron oxide NPs ($D \approx$ 130 nm), which were given to RAW 264.7 and HUVEC cells. Assuming that HepG2, RAW 264.7, and HUVEC cells have a similar protein content, the uptake of the iron oxide NPs coated with a zwitterionic polymer was very close to that of our ZDS-coated NPs. This suggests that the uptake of NPs with zwitterionic coating is scarcely affected by the NP hydrodynamic diameter.

Finally, to investigate the intracellular fate of NPs, we used fluorescent iron oxide NPs coated with a mixture of ZDS and FLC. Confocal imaging of HepG2 exposed to ZDS/FLC-coated NPs again revealed a dose-dependent internalization (Figure 7), with undetectable staining of the plasma membrane

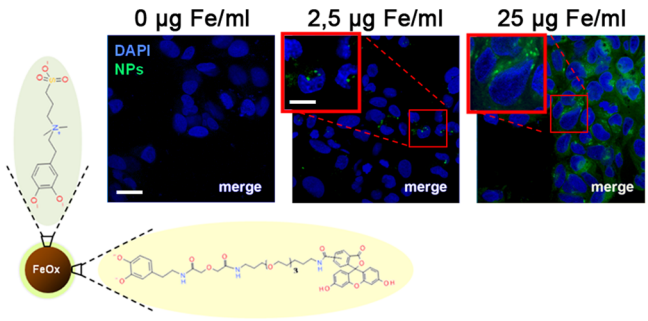

Figure 7. Confocal images of fluorescent NPs (iron oxide NPs coated with a mixture of ZDS and FLC) in HepG2 cells. HepG2 cells were exposed for 24 h to different concentrations of ZDS/FLC-coated NPs and then washed and processed for optical imaging. Scale bar = 20 μm. Inset scale bar = 10 μm. Blue: DAPI staining of cell nuclei; green: GLC staining of NPs.

(Figure 8). Moreover, the higher spatial resolution of fluorescent signals, compared with that of Prussian blue staining, allowed us to identify the intracellular destiny of ZDS/FLC-coated NPs. Fluorescein signals in HepG2 cells, 24 h after the addition of NPs in the medium, colocalized with that of Lysotracker (Figure 8), showing that internalized ZDS/FLC-coated NPs are sent to the lysosomal pathway. Though FLC is longer than ZDS and might have affected the intracellular behavior, this experiment indicates that ZDS-coated NPs should also follow the lysosomal pathway. A similar fate has already been reported for other iron-oxide NPs in cell lines in culture.[42,56−60] The lysosomal destiny of NPs could actually represent a great advantage in cancer therapy as lysosomal-targeted magnetic NPs were recently reported to induce the release of lysosomal content causing cell death upon the action of an alternating magnetic field.[59]

4. CONCLUSIONS

In this study, we synthesized iron oxide NPs coated with ZDS and characterized them in term of coating structure, protein adsorption, cellular toxicity, internalization, and intracellular destiny. We compared them with MEEA-coated NPs prepared from the same batch of nanocrystals, thus differing from ZDS-coated NPs for surface chemistry only. ZDS-coated NPs display a high density of sulfobetaine ligands, which endows the NPs with high stability in complete cell culture medium by preventing NP aggregation or sedimentation and the adsorption of proteins. MEEA-coated NPs are scarcely stable and readily form micrometer-sized aggregates in water. Such

DOI: 10.1021/acs.langmuir.5b01496
Langmuir 2015, 31, 7381−7390

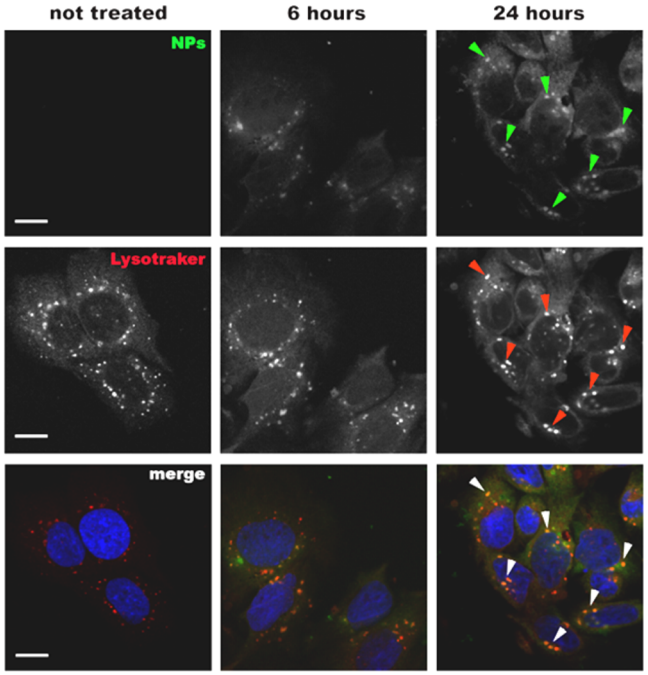

Figure 8. Lysosomal accumulation of fluorescent NPs (iron oxide NPs coated with a mixture of ZDS and FLC) in HepG2 cells. Cells were exposed to these NPs for 6 or 24 h, and then lysosomes were labeled with in vivo Lysotracker staining. Arrowheads indicates sites of colocalization between the green (NPs) and the red signal (Lysotracker). Scale bar = 5 μm.

dramatically different behavior has a profound impact on the in vitro interaction between NPs and cells, affecting cellular toxicity and the efficiency of aspecific internalization. This shows the importance of NP surface chemistry in NP−cell interactions and the necessity of monitoring the NP dispersion during in vitro experiments. ZDS-coated NPs were found to be harmless for an hepatic cell line even at the highest tested concentration (100 μg Fe/mL), whereas MEEA-coated NPs induced cytotoxicity already at 50 μg Fe/mL. The aspecific uptake of NPs in hepatic cells is dose-dependent for both NP types, but it is very low for ZDS-coated NPs. This represents a great advantage when the aim is achieving highly selective targeting via specific NP functionalization. A further advantage of ZDS-coated NPs is their lysosomal intracellular fate, which is desirable when targeted cells are meant to be destroyed, such as in cancer therapy. Taken together, these observations indicate that ZDS-coated NPs could be a good backbone for the development of versatile and specialized NPs suitable for in vivo biomedicine.

■ ASSOCIATED CONTENT

Supporting Information

Synthesis and ligand exchange of NPs; synthesis and FTIR spectra of ligands; characterization techniques; TEM images and ED patterns of NPs; additional DLS experiments; modeling and alternate expression of NP uptake. The Supporting Information is available free of charge on the ACS Publications website at DOI: 10.1021/acs.langmuir.5b01496.

■ AUTHOR INFORMATION

Corresponding Authors

*E-mail: b.chini@in.cnr.it. Fax: +39(0)250316964.

*E-mail: alessandro.ponti@istm.cnr.it. Fax: +39(0)250313927.

Present Address

[⊥]C.D.: Istituto di Chimica Biomolecolare, Consiglio Nazionale delle Ricerche, via P. Gaifami 18, 95126 Catania, Italy.

Author Contributions

[‖]W.M. and M.L. contributed equally to the work.

Notes

The authors declare no competing financial interest.

■ ACKNOWLEDGMENTS

This work has been financially supported by Fondazione CARIPLO (Grant No. 2011-2114) and Regione Lombardia (RSPPTECH Project). We thank Matteo Guidotti (ISTM-CNR) for TGA measurements and Elena Capetti (ISTM-CNR) for assistance in performing DLS experiments.

■ REFERENCES

(1) Krug, H. F.; Wick, P. Nanotoxicology: An Interdisciplinary Challenge. *Angew. Chem., Int. Ed. Engl.* **2011**, *50*, 1260−1278.

(2) *Nanoparticles in Biology and Medicine*; Soloviev, M., Ed.; Methods in Molecular Biology; Humana Press: Totowa, NJ, 2012; Vol. *906*.

(3) Pombo García, K.; Zarschler, K.; Barbaro, L.; Barreto, J. A.; O'Malley, W.; Spiccia, L.; Stephan, H.; Graham, B. Zwitterionic-Coated "Stealth" Nanoparticles for Biomedical Applications: Recent Advances in Countering Biomolecular Corona Formation and Uptake by the Mononuclear Phagocyte System. *Small* **2014**, *10*, 2516−2529.

(4) Choi, H. S.; Liu, W.; Misra, P.; Tanaka, E.; Zimmer, J. P.; Itty Ipe, B.; Bawendi, M. G.; Frangioni, J. V. Renal Clearance of Quantum Dots. *Nat. Biotechnol.* **2007**, *25*, 1165−1170.

(5) Liu, J.; Yu, M.; Zhou, C.; Zheng, J. Renal Clearable Inorganic Nanoparticles: A New Frontier of Bionanotechnology. *Mater. Today* **2013**, *16*, 477−486.

(6) Devadasu, V. R.; Bhardwaj, V.; Kumar, M. N. V. R. Can Controversial Nanotechnology Promise Drug Delivery? *Chem. Rev.* **2013**, *113*, 1686−1735.

(7) Sun, Z.; Yathindranath, V.; Worden, M.; Thliveris, J. a.; Chu, S.; Parkinson, F. E.; Hegmann, T.; Miller, D. W. Characterization of Cellular Uptake and Toxicity of Aminosilane-Coated Iron Oxide Nanoparticles with Different Charges in Central Nervous System-Relevant Cell Culture Models. *Int. J. Nanomed.* **2013**, *8*, 961−970.

(8) Tenzer, S.; Docter, D.; Kuharev, J.; Musyanovych, A.; Fetz, V.; Hecht, R.; Schlenk, F.; Fischer, D.; Kiouptsi, K.; Reinhardt, C.; et al. Rapid Formation of Plasma Protein Corona Critically Affects Nanoparticle Pathophysiology. *Nat. Nanotechnol.* **2013**, *8*, 772−781.

(9) Nel, A. E.; Mädler, L.; Velegol, D.; Xia, T.; Hoek, E. M. V; Somasundaran, P.; Klaessig, F.; Castranova, V.; Thompson, M. Understanding Biophysicochemical Interactions at the Nano-Bio Interface. *Nat. Mater.* **2009**, *8*, 543−557.

(10) Karakoti, A. S.; Das, S.; Thevuthasan, S.; Seal, S. PEGylated Inorganic Nanoparticles. *Angew. Chem., Int. Ed. Engl.* **2011**, *50*, 1980−1994.

(11) Mondini, S.; Drago, C.; Ferretti, A. M.; Puglisi, A.; Ponti, A. Colloidal Stability of Iron Oxide Nanocrystals Coated with a PEG-Based Tetra-Catechol Surfactant. *Nanotechnology* **2013**, *24*, 105702.

(12) Schlenoff, J. B. Zwitteration: Coating Surfaces with Zwitterionic Functionality to Reduce Nonspecific Adsorption. *Langmuir* **2014**, *30*, 9625−9636.

(13) Moyano, D. F.; Saha, K.; Prakash, G.; Yan, B.; Kong, H.; Yazdani, M.; Rotello, V. M. Fabrication of Corona-Free Nanoparticles with Tunable Hydrophobicity. *ACS Nano* **2014**, *No. 7*, 6748−6755.

(14) Kitano, H.; Imai, M.; Sudo, K.; Ide, M. Hydrogen-Bonded Network Structure of Water in Aqueous Solution of Sulfobetaine Polymers. *J. Phys. Chem. B* **2002**, *106*, 11391−11396.

(15) Mornet, S.; Vasseur, S.; Grasset, F.; Duguet, E. Magnetic Nanoparticle Design for Medical Diagnosis and Therapy. *J. Mater. Chem.* **2004**, *14*, 2161.

DOI: 10.1021/acs.langmuir.5b01496
Langmuir 2015, 31, 7381−7390

(16) Ito, A.; Shinkai, M.; Honda, H.; Kobayashi, T. Medical Application of Functionalized Magnetic Nanoparticles. *J. Biosci. Bioeng.* **2005**, *100*, 1−11.
(17) Laurent, S.; Forge, D.; Port, M.; Roch, A.; Robic, C.; Vander Elst, L.; Muller, R. N. Magnetic Iron Oxide Nanoparticles: Synthesis, Stabilization, Vectorization, Physicochemical Characterizations, and Biological Applications. *Chem. Rev.* **2008**, *108*, 2064−2110.
(18) Veiseh, O.; Gunn, J. W.; Zhang, M. Design and Fabrication of Magnetic Nanoparticles for Targeted Drug Delivery and Imaging. *Adv. Drug Delivery Rev.* **2010**, *62*, 284−304.
(19) Xiao, W.; Lin, J.; Li, M.; Ma, Y.; Chen, Y.; Zhang, C.; Li, D.; Gu, H. Prolonged in Vivo Circulation Time by Zwitterionic Modification of Magnetite Nanoparticles for Blood Pool Contrast Agents. *Contrast Media Mol. Imaging* **2012**, *7*, 320−327.
(20) Zhang, L.; Xue, H.; Gao, C.; Carr, L.; Wang, J.; Chu, B.; Jiang, S. Imaging and Cell Targeting Characteristics of Magnetic Nanoparticles Modified by a Functionalizable Zwitterionic Polymer with Adhesive 3,4-Dihydroxyphenyl-L-Alanine Linkages. *Biomaterials* **2010**, *31*, 6582−6588.
(21) Kim, D.; Chae, M. K.; Joo, H. J.; Jeong, I. H.; Cho, J. H.; Lee, C. Facile Preparation of Zwitterion-Stabilized Superparamagnetic Iron Oxide Nanoparticles (ZSPIONs) as an MR Contrast Agent for in Vivo Applications. *Langmuir* **2012**, *28*, 9634−9639.
(22) Rouhana, L. L.; Schlenoff, J. B. Aggregation Resistant Zwitterated Superparamagnetic Nanoparticles. *J. Nanoparticle Res.* **2012**, *14*, 835.
(23) Wei, H.; Insin, N.; Lee, J.; Han, H.-S.; Cordero, J. M.; Liu, W.; Bawendi, M. G. Compact Zwitterion-Coated Iron Oxide Nanoparticles for Biological Applications. *Nano Lett.* **2012**, *12*, 22−25.
(24) Estephan, Z. G.; Hariri, H. H.; Schlenoff, J. B. One-Pot, Exchange-Free, Room-Temperature Synthesis of Sub-10 Nm Aqueous, Noninteracting, and Stable Zwitterated Iron Oxide Nanoparticles. *Langmuir* **2013**, *29*, 2572−2579.
(25) Wei, H.; Bruns, O. T.; Chen, O.; Bawendi, M. G. Compact Zwitterion-Coated Iron Oxide Nanoparticles for in Vitro and in Vivo Imaging. *Integr. Biol.* **2013**, *5*, 108−114.
(26) Zhou, Z.; Wang, L.; Chi, X.; Bao, J.; Yang, L.; Zhao, W.; Chen, Z.; Wang, X.; Chen, X.; Gao, J. Engineered Iron-Oxide-Based Nanoparticles as Enhanced T1 Contrast Agents for Efficient Tumor Imaging. *ACS Nano* **2013**, *7*, 3287−3296.
(27) Peng, X. An Essay on Synthetic Chemistry of Colloidal Nanocrystals. *Nano Res.* **2010**, *2*, 425−447.
(28) Carbone, L.; Cozzoli, P. D. Colloidal Heterostructured Nanocrystals: Synthesis and Growth Mechanisms. *Nano Today* **2010**, *5*, 449−493.
(29) Kim, B. H.; Hackett, M. J.; Park, J.; Hyeon, T. Synthesis, Characterization, and Application of Ultrasmall Nanoparticles. *Chem. Mater.* **2014**, *26*, 59−71.
(30) Soenen, S. J. H.; Brisson, A. R.; Jonckheere, E.; Nuytten, N.; Tan, S.; Himmelreich, U.; De Cuyper, M. The Labeling of Cationic Iron Oxide Nanoparticle-Resistant Hepatocellular Carcinoma Cells Using Targeted Magnetoliposomes. *Biomaterials* **2011**, *32*, 1748−1758.
(31) Liu, Y.; Chen, Z.; Wang, J. Systematic Evaluation of Biocompatibility of Magnetic Fe_3O_4 Nanoparticles with Six Different Mammalian Cell Lines. *J. Nanoparticle Res.* **2010**, *13*, 199−212.
(32) Li, Y.; Chen, Z.; Li, F.; Wang, J.; Zhang, Z. Preparation and in Vitro Studies of MRI-Specific Superparamagnetic Iron Oxide antiGPC3 Probe for Hepatocellular Carcinoma. *Int. J. Nanomed.* **2012**, *7*, 4593−4611.
(33) Qu, J.-B.; Shao, H.-H.; Jing, G.-L.; Huang, F. PEG-Chitosan-Coated Iron Oxide Nanoparticles with High Saturated Magnetization as Carriers of 10-Hydroxycamptothecin: Preparation, Characterization and Cytotoxicity Studies. *Colloids Surf., B* **2013**, *102*, 37−44.
(34) Yathindranath, V.; Sun, Z.; Worden, M.; Donald, L. J.; Thliveris, J. a; Miller, D. W.; Hegmann, T. One-Pot Synthesis of Iron Oxide Nanoparticles with Functional Silane Shells: A Versatile General Precursor for Conjugations and Biomedical Applications. *Langmuir* **2013**, *29*, 10850−10858.
(35) Huang, C.-Y.; Ger, T.-R.; Wei, Z.-H.; Lai, M.-F. Compare Analysis for the Nanotoxicity Effects of Different Amounts of Endocytic Iron Oxide Nanoparticles at Single Cell Level. *PLoS One* **2014**, *9*, e96550.
(36) Déry, J.-P.; Borra, E. F.; Ritcey, A. M. Ethylene Glycol Based Ferrofluid for the Fabrication of Magnetically Deformable Liquid Mirrors. *Chem. Mater.* **2008**, *20*, 6420−6426.
(37) Hyeon, T.; Lee, S. S.; Park, J.; Chung, Y.; Na, H. B. Synthesis of Highly Crystalline and Monodisperse Maghemite Nanocrystallites without a Size-Selection Process. *J. Am. Chem. Soc.* **2001**, *123*, 12798−12801.
(38) Calcagnile, P.; Fragouli, D.; Bayer, I. S.; Anyfantis, G. C.; Martiradonna, L.; Cozzoli, P. D.; Cingolani, R.; Athanassiou, A. Magnetically Driven Floating Foams for the Removal of Oil Contaminants from Water. *ACS Nano* **2012**, *6*, 5413−5419.
(39) Wei, H.; Insin, N.; Lee, J.; Han, H. S.; Cordero, J. M.; Liu, W.; Bawendi, M. G. Compact Zwitterion-Coated Iron Oxide Nanoparticles for Biological Applications. *Nano Lett.* **2012**, *12*, 22−25.
(40) Yoe, J. H.; Jones, A. L. Colorimetric Determination of Iron with Disodium-1,2-Dihydroxybenzene-3,5-Disulfonate. *Ind. Eng. Chem., Anal. Ed.* **1944**, *16*, 111−115.
(41) Yuan, Y.; Rende, D.; Altan, C. L.; Bucak, S.; Ozisik, R.; Borca-Tasciuc, D.-A. Effect of Surface Modification on Magnetization of Iron Oxide Nanoparticle Colloids. *Langmuir* **2012**, *28*, 13051−13059.
(42) Galimard, A.; Safi, M.; Ould-Moussa, N.; Montero, D.; Conjeaud, H.; Berret, J. F. Thirty-Femtogram Detection of Iron in Mammalian Cells. *Small* **2012**, *8*, 2036−2044.
(43) Mondini, S.; Ferretti, A. M.; Puglisi, A.; Ponti, A. Pebbles and PebbleJuggler: Software for Accurate, Unbiased, and Fast Measurement and Analysis of Nanoparticle Morphology from Transmission Electron Microscopy (TEM) Micrographs. *Nanoscale* **2012**, *4*, 5356−5372.
(44) Pigorsch, E. Spectroscopic Characterisation of Cationic Quaternary Ammonium Starches. *Starch - Stärke* **2009**, *61*, 129−138.
(45) Shen, L.; Laibinis, P. E.; Hatton, T. A. Bilayer Surfactant Stabilized Magnetic Fluids: Synthesis and Interactions at Interfaces. *Langmuir* **1999**, *15*, 447−453.
(46) Kwon, E. E.; Castaldi, M. J. Mechanistic Understanding of Polycyclic Aromatic Hydrocarbons (PAHs) from the Thermal Degradation of Tires under Various Oxygen Concentration Atmospheres. *Environ. Sci. Technol.* **2012**, *46*, 12921−12926.
(47) Ni, K.; Zhou, X.; Zhao, L.; Wang, H.; Ren, Y.; Wei, D. Magnetic Catechol-Chitosan with Bioinspired Adhesive Surface: Preparation and Immobilization of ??-Transaminase. *PLoS One* **2012**, *7*, 1−8.
(48) Nabid, M. R.; Zamiraei, Z.; Sedghi, R.; Nazari, S. Synthesis and Characterization of Poly(catechol) Catalyzed by Porphyrin and Enzyme. *Polym. Bull.* **2010**, *64*, 855−865.
(49) Han, H.-S.; Martin, J. D.; Lee, J.; Harris, D. K.; Fukumura, D.; Jain, R. K.; Bawendi, M. Spatial Charge Configuration Regulates Nanoparticle Transport and Binding Behavior in Vivo. *Angew. Chem., Int. Ed. Engl.* **2013**, *52*, 1414−1419.
(50) Safi, M.; Courtois, J.; Seigneuret, M.; Conjeaud, H.; Berret, J. F. The Effects of Aggregation and Protein Corona on the Cellular Internalization of Iron Oxide Nanoparticles. *Biomaterials* **2011**, *32*, 9353−9363.
(51) Provencher, S. W. A Constrained Regularization Method for Inverting Data Represented by Linear Algebraic or Integral Equations. *Comput. Phys. Commun.* **1982**, *27*, 213−227.
(52) Soenen, S. J. H.; De Cuyper, M. Assessing Cytotoxicity of (Iron Oxide-Based) Nanoparticles: An Overview of Different Methods Exemplified with Cationic Magnetoliposomes. *Contrast Media Mol. Imaging* **2009**, *4*, 207−219.
(53) Mahmoudi, M.; Hofmann, H.; Rothen-Rutishauser, B.; Petri-Fink, A. Assessing the in Vitro and in Vivo Toxicity of Superparamagnetic Iron Oxide Nanoparticles. *Chem. Rev.* **2012**, *112*, 2323−2338.
(54) Laurent, S.; Burtea, C.; Thirifays, C.; Häfeli, U. O.; Mahmoudi, M. Crucial Ignored Parameters on Nanotoxicology: The Importance

DOI: 10.1021/acs.langmuir.5b01496
Langmuir 2015, 31, 7381−7390

of Toxicity Assay Modifications and "Cell Vision. *PLoS One* **2012**, *7*, e29997.
(55) Jiang, W.; Lai, K.; Wu, Y.; Gu, Z. Protein Corona on Magnetite Nanoparticles and Internalization of Nanoparticle-Protein Complexes into Healthy and Cancer Cells. *Arch. Pharm. Res.* **2014**, *37*, 129−141.
(56) Goya, G. F.; Marcos-Campos, I.; Fernández-Pacheco, R.; Sáez, B.; Godino, J.; Asín, L.; Lambea, J.; Tabuenca, P.; Mayordomo, J. I.; Larrad, L.; et al. Dendritic Cell Uptake of Iron-Based Magnetic Nanoparticles. *Cell Biol. Int.* **2008**, *32*, 1001−1005.
(57) Lai, C.-H.; Lin, C.-Y.; Wu, H.-T.; Chan, H.-S.; Chuang, Y.-J.; Chen, C.-T.; Lin, C.-C. Galactose Encapsulated Multifunctional Nanoparticle for HepG2 Cell Internalization. *Adv. Funct. Mater.* **2010**, *20*, 3948−3958.
(58) Gu, J.; Xu, H.; Han, Y.; Dai, W.; Hao, W.; Wang, C.; Gu, N.; Xu, H.; Cao, J. The Internalization Pathway, Metabolic Fate and Biological Effect of Superparamagnetic Iron Oxide Nanoparticles in the Macrophage-like RAW264.7 Cell. *Sci. China Life Sci.* **2011**, *54*, 793−805.
(59) Domenech, M.; Marrero-Berrios, I.; Torres-Lugo, M.; Rinaldi, C. Lysosomal Membrane Permeabilization by Targeted Magnetic Nanoparticles in Alternating Magnetic Fields. *ACS Nano* **2013**, *7*, 5091−5101.
(60) Fröhlich, E. Cellular Targets and Mechanisms in the Cytotoxic Action of Non-Biodegradable Engineered Nanoparticles. *Curr. Drug Metab.* **2013**, *14*, 976−988.

DOI: 10.1021/acs.langmuir.5b01496
Langmuir 2015, 31, 7381−7390